Progress In Electromagnetics Research B, Vol. 40, 279–303, 2012

SEASONAL ANALYSIS AND PREDICTION OF RAINFALL EFFECTS IN EASTERN SOUTH AFRICA AT MICROWAVE FREQUENCIES

A. A. Alonge* **and T. J. Afullo**

School of Electrical, Electronics and Computer Engineering, University of KwaZulu-Natal, Durban 4041, South Africa

Abstract—Network fade countermeasures for link budget can be better implemented based on the knowledge of seasonal variability of rainfall attenuation in a locality. Therefore, in this study, a seasonal approach is applied to estimate the effects of spatial rainfall attenuation in Durban (29°52'S, 30°58'E), South Africa using two-year rainfall data obtained from the RD-80 Joss-Waldvogel (J-W) distrometer. An analysis is undertaken for different seasons to obtain the rainfall rate exceedences at 0.001%, 0.01%, 0.1% and 1% of time. Consequently, rainfall drop-size distribution (DSD) models are developed for the control site at different seasons for the same period. The probability density analysis for each model indicates that the lognormal distribution best fits the summer and autumn season with percentage root-mean-square errors (RMS) of 30% and 26% respectively; gamma distribution fits winter season with RMS error of 16% and Weibull distribution fits spring season with RMS error of 26%. The results from the rainfall rate and rainfall DSD are combined to estimate the rainfall specific attenuation, by applying spherical droplet assumption for Mie scattering techniques, between 2 GHz and 1000 GHz. With this, the seasonal k and α coefficients for specific attenuation are derived from the best rainfall DSD models, using regression technique at 2.5 GHz, 25 GHz, 40 GHz and 100 GHz. At these frequencies, the results show that the predicted specific attenuation coefficients for all seasonal rainfall rates at the control site are lower, when compared to those from ITU-R models. It is concluded that specific attenuation levels may be similar and more intense in summer and autumn seasons, while, lower and less intense in autumn and winter seasons at similar rainfall rates.

Received 3 February 2012, Accepted 17 April 2012, Scheduled 27 April 2012

* Corresponding author: Akintunde Alonge (dtanthony740@gmail.com).

1. INTRODUCTION

Rainfall attenuation is a significant consideration in link budget particularly as the terrestrial or satellite link design frequency exceeds the 10 GHz threshold and beyond [1–3]. Authors have attributed the significance of rainfall attenuation to the spatial non-homogeneity of rainfall droplets, which usually result in absorption and scattering of propagated signals [3–5]. Although, worldwide approaches have been recommended by ITU-R in their rainfall design templates available in [6–8], there persists a problem of exactness and suitability since rainfall is dependent on climatic variation around the world. Apart from climatic dependence, the prediction of rainfall attenuation using ITU-R model(s) is primarily based on the assumption of uniform rainfall water volume for every part of the world (as seen in the values of k and α in ITU-R P.838-3 [6]). Rainfall water volume is a regional factor, specifically dependent on local seasonal cycle, thereby, producing variability in the seasonal distribution of rainfall attenuation in a locality [9, 10]. Since seasonal cycles are of universal variability — different climatic conditions are therefore experienced in various regions; therefore, water volume is not constant around the world. The consequence of this, is that, the ITU-R estimates are often found to over-estimate or under-estimate rainfall attenuation at different parts of the world. This has been confirmed in a number of microwave studies especially at tropical, equatorial and subtropical zones [1, 3, 11, 12].

Meanwhile, the subject of this paper is on the seasonal effects of rainfall attenuation in Durban, a coastal city located along the Eastern frontiers of the Republic of South Africa. With an average annual precipitation of over 1000 mm, Durban is unarguably one of the wettest cities in South Africa [13]. Besides, the convective effects of the Agulhas currents from the Indian ocean, allows for a warmer climate throughout the year when compared with other South African cities [14]. The city is credited with an annual cycle of four seasons, which determine the yearly variation of precipitation, and they are described by Fashuyi et al. [15]: Summer (mid-October to mid-February), Autumn (mid-February to April), Winter (May to July), and, Spring (August to mid-October).

Rainfall research involving the city of Durban undertaken in [15] applied five year data from the South African Weather Service (SAWS) database in 2004. The study attempted to establish the cumulative distributions of several control sites in South Africa, of which Durban is included. The city was observed to have the second highest rainfall intensity besides Richards Bay, indicating the huge presence of hydrometeor-induced attenuation. Further studies on rainfall

attenuation in Durban [9, 16], focusing mainly on seasonal attenuation studies, were conducted at 19.5 GHz via 6.73 km microwave link between two campuses of the University of KwaZulu-Natal, Durban. It was noted that the control site experiences varying degrees of rainfall attenuation during its annual cycle of four seasons. For instance, [9, 15] noted that the seasons of summer and autumn are responsible for a substantial amount of rainfall attenuation in most South African cities, with the exception of Cape Town. This observation has led to the suggestion, that large fade margins be made available for these seasons especially cities in these category, except those around the Western-Cape provinces. The Western-Cape province, has been identified by authors [9, 17] as being characterised by Mediterranean climate, largely because the influence of the predominantly cold Atlantic ocean currents and loosely warm Indian ocean currents.

Rainfall attenuation studies in Durban have mainly been approached based on two microstructural parameters namely, rainfall rate and rain drop-sizes [9, 15–21]. While the ITU-R P.837 [8] climatic maps have proved useful for link designs, recent studies in Durban [17, 22] have shown that rainfall rate prediction appear to favour gamma probability distribution patterns. In addition, rainfall patterns appear to have a high population of samples within the drizzle rainfall types, with thunderstorm rainfall types having the least number of samples [22]. Afullo [19] observed that thunderstorms rainfall above 30 mm/h mainly appear in autumn and summer seasons, thereby suggesting that fewer thunderstorm samples exists in winter and spring seasons. With respect to rainfall drop-sizes, Odedina and Afullo [20] showed that rainfall DSD models with lognormal and modified gamma structures gave better fitting to the point rainfall measurements in Durban. In lieu of this, attempts have been made by Afullo [19] and Owolawi [21] to develop lognormal DSD models for the control sites using different models and techniques. Alonge and Afullo [18] also developed regime-based lognormal DSD models for four distinct rainfall regimes in Durban namely: drizzle, widespread, shower and thunderstorm.

Interestingly, it appears that little concern have been paid to the seasonal variation of rainfall rate in Durban, this is fully explored in this paper. The seasonal approach in this study is undertaken using two year point rainfall measurement from the J-W distrometer acquired over a period of two years at our control site in Durban. The collected data is examined for rainfall rate and rainfall DSD variations on a seasonal period. The results from the rainfall analysis are further modified, to predict rainfall specific attenuation for frequencies between 2 GHz and 1000 GHz, using Mie spherical droplet assumption.

2. MEASUREMENT AND DATA PROCESSING

In this study, the J-W RD-80 impact distrometer is used for the measurement of rainfall microstructural parameters. The equipment is installed at the School of Electrical, Electronics and Computer Engineering, at the Howard College Campus, University of KwaZulu-Natal, Durban at spatial coordinates of longitude 29°52'S and latitude 30°58'E at a vertical height of 139.7 m above sea level. The equipment is designed and manufactured by Distromet Ltd., Switzerland with the capability of measuring rainfall rate, rainfall drop-size and radar reflectivity [23]. The equipment architecture has three components — indoor, outdoor and archiving units — with a measuring accuracy of ±5%. It has 20 independent bins for recording at one minute sampling time, different categories of rain drops with diameter classes ranging from 0.359 mm to 5.373 mm. The computations for rainfall rate and rainfall DSD from the distrometer are both made available in (1) and (2) given by [24] as:

$$R = \frac{6\pi \times 10^{-4}}{A \times T} \sum_{i=1}^{20} C_i \, D_i^3 = \sum_{i=1}^{20} R_i \, [\mathrm{mm/h}] \tag{1}$$

$$N(D_i) = \frac{C_i}{A \times T \times v(D_i) \times \Delta D_i} \left[\mathrm{m^{-3}mm^{-1}}\right] \tag{2}$$

where C_i represents the number of rain drops present at diameter class, i; D_i is the mean of the diameter class, i; A is the sampling area of the distrometer surface given as $0.005\,\mathrm{m}^2$; T is the sampling time given as 60 seconds; ΔD_i is the diameter interval between two successive classes, i and $(i+1)$.

The rainfall measurements were taken over a period of two years between January 2009 and December 2010, although a few instances of equipment outages were experienced. It should be noted that the highest rainfall rate recorded at our site was 117.15 mm/h with a total of 48, 194 filtered rainfall samples. The effects of dead-time errors was compensated for by removing rainfall samples with overall sum of drops less than 10. Table 1 gives the seasonal statistics for the processed rainfall data in Durban.

3. SEASONAL VARIATION OF RAINFALL RATE

While microwave link design is mainly concerned with the 99.9% system availability, the knowledge of the percentage of time rainfall rate is exceeded (also known as $R_{0.01}$) is a useful index. Based on the processed rainfall data, the monthly values of $R_{0.01}$ were obtained from

Table 1. Rainfall statistics in Durban based on Seasonal Cycles.

SEASON	Number of Samples	Maximum Rainfall Rate (mm/h)	Total rainfall time (hours)	Percentage of Group Data (%)
Summer	22769	57.67	379.5	47.25
Autumn	8995	117.15	149.92	18.67
Winter	3878	76.43	64.63	8.05
Spring	12552	20.37	209.2	26.03

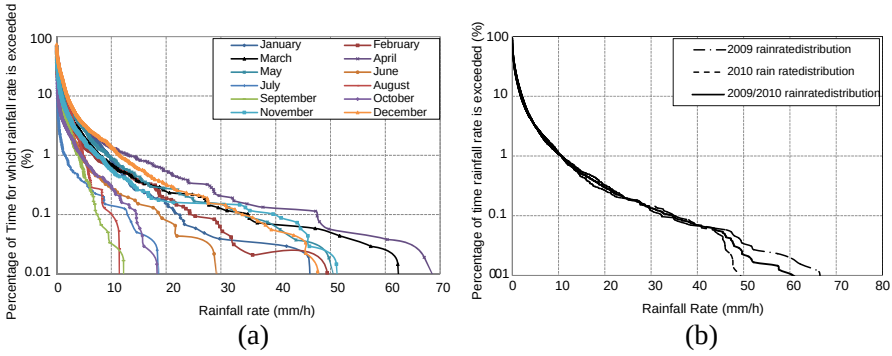

Figure 1. Monthly and annual distribution of rainfall rate between 2009 and 2010. (a) Monthly variation of $R_{0.01}$ in Durban for the period of measurement. (b) Annual rainfall rate distribution in Durban in 2009 and 2010.

the two year measurement in Durban. Figures 1(a) and 1(b) show the monthly rain rate distribution and annual rain rate distribution respectively. The trend of the monthly values of $R_{0.01}$ at our site is taken as being *double maxima* or *bimodal* in shape with the first peak occurring at the threshold of autumn (usually around April). $R_{0.01}$ is seen to gradually rise in summer from January and attains its first peak in April, and then gradually relapses, with the lowest values around the winter months of August and September. However, the value slowly rises from the month of October, with second peak at November, and, December and January having a similar back-to-back $R_{0.01}$ value for the season of summer. Generally, the four months of winter, spilling into September in spring season witness the lowest rainfall rates. It is observed that the four seasons in Durban are dependent on the monthly variations in rainfall. Since rainfall attenuation is directly related to rainfall rate, it is obvious that the first five months and the last two

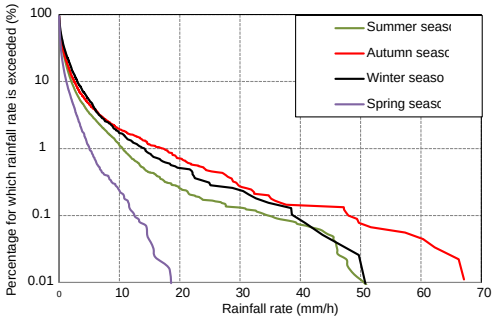

Figure 2. Seasonal distribution of rainfall rate in Durban between 2009 and 2010.

Table 2. Seasonal statistics on rainfall rate exceeded in Durban for the period of measurement.

SEASON	**Rainfall rate**	**Time for which rainfall rate is exceeded (%)**			
		1	**0.1**	**0.01**	**0.001**
SUMMER	(mm/h)	10.52	34.64	50.48	56.42
AUTUMN		17.18	47.98	72.15	112.65
WINTER		14.15	38.88	53.37	75.40
SPRING		5.025	12.52	18.51	20.14

months of the calendar year will witness larger effects of rain fading for microwave networks.

The seasonal distribution of rainfall rate for the same period of measurement is presented in Figure 2. The graph here shows that for our site, the season of autumn has the highest seasonal value of $R_{0.01}$, this is followed by the seasons of summer, spring and winter accordingly. From the set of graphs provided in Figure 1, it is observed that the rainfall rate exceedences for autumn season at $R_{0.01} = 72.15\,\text{mm/h}$ is the highest. The suspect here might be the result of the overlapping seasonal transition between the summer and autumn season in the month of April. The seasons of summer and winter are also observed to have closer values of $R_{0.01}$ at 50.48 mm/h and 53.37 mm/h respectively. The season of spring has the lowest $R_{0.01}$ at 18.51 mm/h. Table 2 shows the summary of the respectively seasonal values of rainfall rate at 0.001%, 0.01%, 0.1% and 1% percentage of time respectively. Even though the winter season has a high $R_{0.01}$ value, it does appear that rainfall occurrences are not generally high

Table 3. Rainfall regime statistics for different seasons in Durban.

SEASON	NUMBER OF SAMPLES			
	DRIZZLE	WIDESPREAD	SHOWER	THUNDERSTORM
SUMMER	22003	510	239	17
AUTUMN	8584	235	163	13
WINTER	3673	139	62	4
SPRING	12424	98	30	N/A

during winter as can be seen in Table 1. Also, there are fewer rainfall samples at high rainfall rates suggesting the preponderance of low rainfall rate samples. When compared with winter season, summer has more rainfall samples with high rainfall rates, and therefore, will suffer more from intense rainfall attenuation. The low rainfall rates experienced in spring may be due to the spill-over effects of the winter for the period of measurement. The seasonal distribution of rainfall in Durban seem to suggest rainfall attenuation usually peaks at months closer to the onset of winter, this has earlier been verified in the study of Odedina and Afullo [9].

4. SEASONAL PROMINENCE OF RAINFALL REGIMES

The nature of rainfall types is a determinant factor in examining the rainfall structures for each seasons in Durban. One interesting method of observing rainfall structures is by grouping the collected data into specified rainfall regimes. For easy referencing, four rainfall regimes are considered as discussed by previous authors [12, 26]: drizzle ($R < 5\,\mathrm{mm/h}$), widespread ($5\,\mathrm{mm/h} \leq R \leq 10\,\mathrm{mm/h}$), shower ($10\,\mathrm{mm/h} \leq R \leq 40\,\mathrm{mm/h}$) and thunderstorm ($R > 40\,\mathrm{mm/h}$).

Using the available data from the rainfall measurements, these rainfall regimes are considered for each season as seen in Table 3. The summer season is noted to have the highest number of samples for all regimes, followed by autumn, winter and spring seasons in descending order respectively. In spring season, for example, rainfall samples for thunderstorm regime are totally absent. By obtaining the probability density function (PDF) for the average rain drop-size per regime for each season, a comparative analysis was undertaken on the rainfall structures for the prevailing seasons. The results are shown in Figures 3(a)–(d).

Figure 3(a) shows the PDFs of drizzle rainfall regimes for different seasons; all the plots have a unimodal shapes. It is observed that the shape and scale profiles for summer, autumn and spring season are

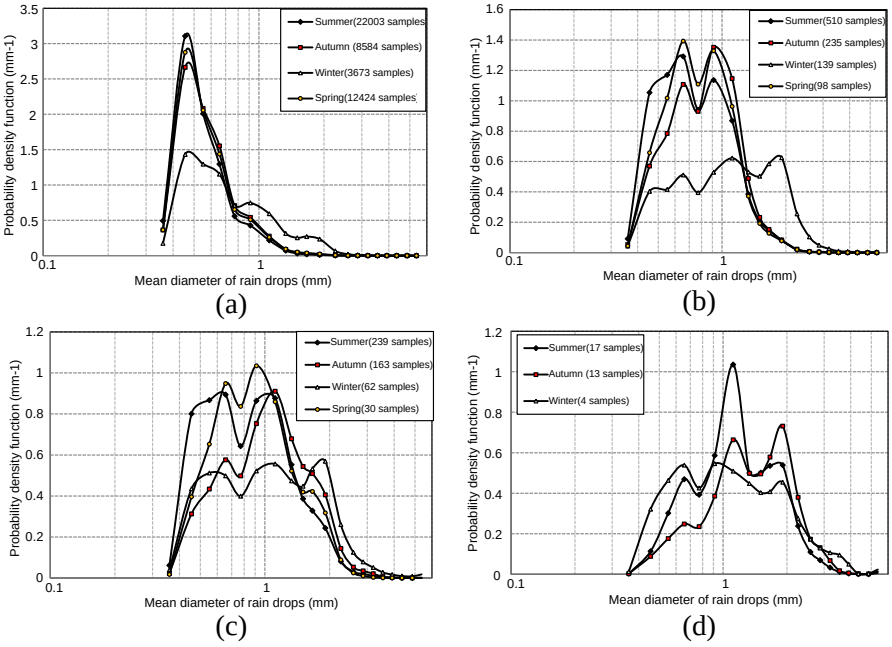

Figure 3. Probability density function plots showing rainfall regime prominence for seasonal cycle in Durban. (a) Drizzle rainfall regime ($R < 5\,\mathrm{mm/h}$). (b) Widespread rainfall regime ($5\,\mathrm{mm/h} \leq R \leq 10\,\mathrm{mm/h}$). (c) Shower rainfall regime ($10\,\mathrm{mm/h} \leq \mathrm{R} \leq 40\,\mathrm{mm/h}$). (d) Thunderstorm rainfall regime ($R > 40\,\mathrm{mm/h}$).

similar. The similarities in the shape and scale profile may indicate that the rainfall distribution structures for drizzle regimes for these seasons may significantly be similar in Durban. The PDF plots for these seasons, show that they significantly peak at 0.45 mm, suggesting that majority of the raindrops are within this diameter. Meanwhile, the summer season is observed to have the highest peak density, followed by the spring and autumn season. The winter season with peak density at 0.45 mm is the lowest, among all the seasons, albeit with larger diameter raindrops.

For widespread rainfall regimes, their average PDFs for different season are shown in Figure 3(b). As in the previous case of drizzle rainfall, the three seasons of summer, autumn and spring have similar PDF shape and scale profiles. However, the shape profiles for these seasons are observed to be bimodal with peaks at 0.65 mm and 0.9 mm raindrop mean diameter. The bimodality observed may be as a result

'shifting' raindrop diameter population due to overlapping rainfall regimes, particularly in transition from drizzle regime to widespread regime. In the first peak of the bimodal section, the spring and autumn seasons have the highest and lowest PDF peaks respectively. On the other hand, in the second peak, the reverse is the case with autumn having the highest peak. Also in this regime, the winter season has the lowest peak in comparison to other seasons, with an amorphous spread. It is also observed that the winter season unlike other seasons, has an appreciable PDF beyond 1.5 mm raindrop diameter bound. This indicates that large rainfall drops exist for widespread rainfall during winter season.

A deviation in the average seasonal PDF pattern is observed for shower rainfall regimes as shown in Figure 3(c). Prominent bimodal shape profiles are also observed for spring and summer seasons with the spring season having a higher PDF peaks. The locations of the first and second PDF peaks for summer and spring seasons are centred around 0.65 mm and 0.93 mm diameter bound respectively (small rainfall droplets). Unimodal and amorphous peaks are also observed for autumn and winter seasons respectively, though, the autumn season exhibits a higher peak density. The autumn seasonal PDF is skewed right with the peaks at 1.3 mm diameter bound. The winter season, however, is observed to have PDF peaks around 0.55 mm, 1.3 mm and 1.9 mm possessing higher drop-size densities closer to 2 mm diameter bound.

For thunderstorm rainfall regimes in Figure 3(d), the average PDF of the summer season in unimodal with peaks at around 1.3 mm and considerable raindrop densities up to 2 mm. The autumn season has bimodal peaks at around 1.3 mm and 1.9 mm, with lower drop densities than the summer season. The winter season has amorphous peaks with the lowest seasonal peak densities at 0.65 mm, 0.95 mm and 1.9 mm diameter bound. It is observed that the spring season experiences no occurrence of thunderstorm rainfall suggesting that no rainfall rates above 40 mm/h exist. This is possible because the spring season suffers greatly from the after-effects of the winter 'dry' spell than other seasons in Durban.

In summary, it is noted that the average rain drop-size PDF structures in Durban for rainfall rates up to 10 mm/h (drizzle and widespread rains) may be similar for summer, autumn and spring seasons. However, winter season possesses a different PDF structure within these rainfall regimes, but have larger raindrops instead. For rainfall rates above 10 mm/h (shower and thunderstorm rains), the PDF structures are obviously different for all seasons with preponderance in the number of large raindrops.

5. DEVELOPMENT OF SEASONAL RAINFALL DSD FOR DURBAN, SOUTH AFRICA

The development of rainfall DSD from the seasonal data is an important step towards achieving the prediction of rainfall attenuation at our control site. Thus, statistical models are applied to develop appropriate functions which describe the rainfall DSD pattern in Durban. For the purpose of this study, three statistical distributions are considered: lognormal, modified gamma and Weibull distribution models. These models are utilized, firstly, because contemporary authors [18–21] have recommended the first two models as appropriate for our subtropical location. Secondly, similar research around the world for tropical regions has found the first two distributions as good models especially at high rainfall rates [12, 25–27].

Equations (3), (4) and (5) represent the functions for the various models under consideration. The 2-parameter for rainfall DSD lognormal model is defined from Ajayi et al. [25, 26] as:

$$N(D_i) = \frac{N_T}{\sigma D_i \sqrt{2\pi}} \exp\left[-0.5\left(\frac{\ln(D_i) - \mu}{\sigma}\right)^2\right] \left[\mathrm{m}^{-3}\mathrm{mm}^{-1}\right] \quad (3)$$

where N_T is the concentration of rain drops per unit volume, μ and σ are the mean and standard deviation of the drop-sizes respectively. All the estimators are given as a function of rainfall rate as found in most literatures.

The 3-parameter modified gamma model for rainfall DSD is given by [28, 29] as:

$$N(D_i) = N_m D_i^{\mu} \exp(-\Lambda D_i) \left[\mathrm{m}^{-3}\mathrm{mm}^{-1}\right] \quad (4)$$

where N_m is the scaling due to the number of rainfall drops, μ and Λ are both the shape and slope parameters of the distribution respectively. As usual, the estimators are parameterized as a function of rainfall rate.

The 3-parameter Weibull rainfall DSD model, initially proposed by [30, 31] is given by:

$$N(D_i) = N_w \left(\frac{\beta}{\gamma}\right)\left(\frac{D_i}{\gamma}\right)^{\beta-1} \exp\left[-\left(\frac{D_i}{\gamma}\right)^{\beta}\right] \left[\mathrm{m}^{-3}\mathrm{mm}^{-1}\right] \quad (5)$$

where N_w is again the scaling to rainfall drops, β and γ represent the shape and scale parameters of the Weibull probability distribution parameterized as a function of rainfall rate.

To get a stable relationship between these estimators and rainfall rates, a suitable point estimation technique is employed to derive appropriate rainfall DSD functions. This is explored in the next section.

6. METHOD OF MOMENTS POINT ESTIMATION TECHNIQUE

Numerous point estimation techniques exist for the derivation of point estimators related to statistical models [12]. Examples of such techniques include the method of maximum likelihood (ML), Bayesian estimation, method of moments (MM or MoM) and Kernel estimation. The biweight Kernel estimation, for example, has been recently applied by Afullo [19] in his annual studies of rainfall DSD in Durban. However, for this study, the method of moment is used for point estimation as applied by previous researchers in rainfall attenuation studies [12, 25, 32].

In this method of rainfall DSD estimation, the nth moment function for a discrete value of the random variable, D_i, as given by Ajayi and Olsen [25] is:

$$M_n = \sum_{i=1}^{N} D_i^n N(D_i) \Delta D_i \tag{6}$$

where D_i is the diameter of the raindrops for N discrete samples, $N(D_i)$ is the rain drop-size distribution for N discrete number of rainfall samples and ΔD_i is the diameter interval between successive rainfall drop sizes. In this case, $N = 20$, corresponding to the total number of distrometer channels.

Equation (6) represents the nth moment obtained directly from the distrometer measurements. This technique is reportedly related to other microwave rainfall attenuation indices such as liquid water content, rainfall attenuation, rainfall rate [12, 25–27, 32]. The resulting moment estimators are fitted with the rainfall samples using regression techniques.

The moment function generator for a lognormal DSD is given as:

$$M_n = N_T \exp\left[n\mu + \frac{1}{2}(n\sigma)^2\right] \tag{7}$$

The third, fourth and sixth moments are considered sufficient to derive the input parameters N_T, μ and σ for the lognormal moment as suggested in [12, 27, 32]. The solutions to these three selected moments according to [7] are:

$$N_T = \exp\left[(24L_3 - 27L_4 + 6L_6)/3\right] \tag{7a}$$

$$\mu = (-10L_3 + 13.5L_4 - 3.5L_6)/3 \tag{7b}$$

$$\sigma^2 = (2L_3 - 3L_4 + L_6)/3 \tag{7c}$$

In the above equations, the values of L_3, L_4 and L_6 represent the natural logarithms of the measured moments M_3, M_4 and M_6.

The modified gamma model has its moment function given by:

$$M_n = N_m \frac{\Gamma(\mu + n + 1)}{\Lambda^{\mu+n+1}} \tag{8}$$

The moments considered here are also the third, fourth and sixth moments. The solution to the theoretical moments for the modified gamma is given in [32] as:

$$\mu = \frac{11F - 8 + \sqrt{F\,(F+8)}}{2\,(1-F)}; F = \frac{M_4^3}{M_3^2 M_6} \tag{8a}$$

with,

$$\Lambda = (\mu + 4)\, M_3/M_4 \tag{8b}$$

$$N_m = \Lambda^{\mu+4} M_3/\Gamma\,(\mu + 4) \tag{8c}$$

As seen from (8a), (8b) and (8c), the first two moments, M_3 and M_4, are sufficient to estimate the parameters of Λ and thus, N_m (concentration) provided that μ assumes a fixed constant.

The Weibull moment function is given by Murthy et al. [33]:

$$M_n = N_w \gamma^n \Gamma\left(1 + \frac{\gamma}{\beta}\right) \tag{9}$$

Our solution for the three unknown parameters N_w, γ and β for the third, fourth and sixth moments are given as:

$$\beta = -\frac{0.7067}{\ln(\varphi)}; \quad \varphi = \frac{0.9186 M_4^3}{M_3^2 \cdot M_6} \tag{9a}$$

$$\gamma = \frac{0.8660 M_4}{M_3} \times (0.2867\beta)^{\frac{1}{\beta}} \tag{9b}$$

$$N_w = \frac{0.2303 M_3 \beta^{\left(\frac{\beta+6}{2\beta}\right)}}{\gamma^3\,(1.3443)^{\frac{1}{\beta}}} \tag{9c}$$

7. SEASONAL VARIATION OF RAINFALL DSD

The results obtained for the seasonal DSDs for the city of Durban using the method of moment estimation technique are presented in Table 4. The seasonal classification in South Africa earlier been discussed in the introduction is used to group the rainfall data for the city of Durban. The statistics for seasonal classification are available in Table 2.

In Table 4, the season of summer is observed to have the highest rain drop concentration with N_{T}, N_m and N_{w} for all the proposed

models having high coefficients. The season of winter, on the other hand, has the lowest rain drop concentration indicating a low volume of rainfall water for that period. A closer look at the results in Table 4 from the lognormal model show that the ranking of seasons with high coefficients of N_T as follows in descending order: summer, autumn, spring and winter. Again, the effect of sparse rainfall occurrences is evident in winter season as the coefficients are much lower compared with those other seasons. The coefficients of mean, μ, for autumn and spring season are seen to be closer but different from the lower coefficients observed in summer season. On the other hand, the coefficients of σ^2 for summer and spring season are seen to be closer, as are those of autumn and winter season. For the Weibull model in Table 4, the scaling parameter, N_w, follow the order of ranking as previously observed in lognormal model. The shape parameter, β, is seen to be closer for the seasons of summer, autumn and spring based on their power-law coefficients. In addition, the scale parameter, γ, for the seasons of autumn and spring are also found to be close; winter season has higher coefficients than summer season. For the modified

Table 4. Model parameters for different rainfall DSD statistical models for seasonal analysis in Durban, South Africa.

	LOGNORMAL DSD MODEL		
Seasons	$\boldsymbol{N_T}$	$\boldsymbol{\mu}$	$\boldsymbol{\sigma^2}$
Summer	$376.7R^{0.4505}$	$-0.416 + 0.116\ln(R)$	$0.0816 + 0.0125\ln(R)$
Autumn	$239.13R^{0.3752}$	$-0.2671 + 0.1454\ln(R)$	$0.0667 + 0.0081\ln(R)$
Winter	$35.78R^{0.163}$	$0.2467 + 0.2163\ln(R)$	$0.0611 + 0.003\ln(R)$
Spring	$155.6R^{0.4077}$	$-0.1922 + 0.1338\ln(R)$	$0.0849 + 0.0099\ln(R)$
	WEIBULL DSD MODEL		
Seasons	$\boldsymbol{\beta}$	$\boldsymbol{\gamma}$	$\boldsymbol{N_w}$
Summer	$2.5048R^{-0.153}$	$0.616R^{0.1014}$	$571.78R^{0.4677}$
Autumn	$2.8453R^{-0.11}$	$0.7438R^{0.1404}$	$345.78R^{0.3806}$
Winter	$3.0063R^{-0.046}$	$1.2564R^{0.2162}$	$51.78R^{0.1622}$
Spring	$2.3298R^{-0.121}$	$0.7799R^{0.1234}$	$233.43R^{0.4211}$
	MODIFIED GAMMA DSD MODEL		
Seasons	$\boldsymbol{\mu}$	$\boldsymbol{N_m}$	$\boldsymbol{\Lambda}$
Summer	2	$1.32 \times 10^5 R^{-0.103}$	$6.8345R^{-0.16}$
Autumn	2	$6.8944 \times 10^4 R^{-0.194}$	$6.2056R^{-0.174}$
Winter	2	$2420.9R^{-0.535}$	$3.7854R^{-0.227}$
Spring	2	$2.6524 \times 10^4 R^{-0.156}$	$5.4019R^{-0.168}$

gamma model in Table 4, all seasons are observed to take different values of coefficients for the scaling parameter, N_m. However, the coefficients of the slope parameter, Λ, are found to be closer for summer and autumn seasons, with those of winter season being the lowest. A general trend in all these models is the close values of statistical parameters for summer and autumn seasons, suggesting again strong similarities in the rainfall patterns and structures in these seasons. The winter season is mostly found to have the dissimilar statistical coefficients irrespective of the model applied.

The plotted graphs from the results are shown in Figures 4(a)–(d) with the different DSD variation for different seasons in Durban. The estimated DSD for summer season at $R_{0.01} = 56.42\,\text{mm/h}$ has a maximum peak at $2000\,\text{m}^{-3}\text{mm}^{-1}$; autumn season with $R_{0.01} = 72.15\,\text{mm/h}$ has a DSD closer to $2000\,\text{m}^{-3}\text{mm}^{-1}$. Although, summer and autumn, have close DSD peaks, they do not however coincide at

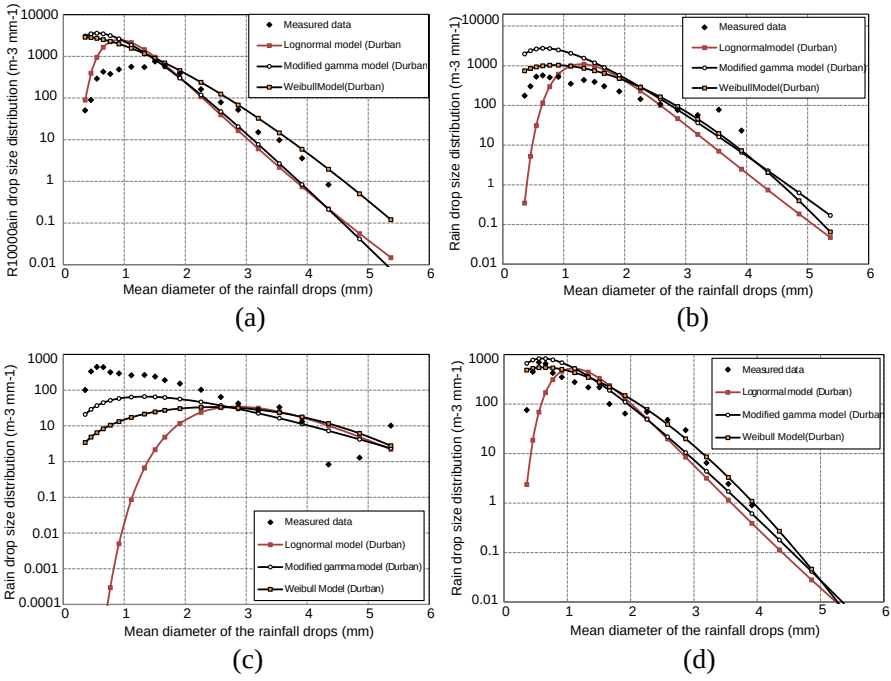

Figure 4. Rainfall DSD in Durban for different seasons using the proposed models. (a) Summer season with $R_{0.01} = 56.42\,\text{mm/h}$. (b) Autumn season with $R_{0.01} = 72.15\,\text{mm/h}$. (c) Winter season with $R_{0.01} = 53.37\text{mm/h}$. (d) Spring season with $R_{0.01} = 18.51\,\text{mm/h}$.

the same diameter bound. For example, at $R_{0.01}$, Autumn DSD peak occurs at 1.331 mm bound, while the summer DSD peak occurs at 0.771 mm bound. This suggests that the autumn season have raindrops of larger diameter than the summer season for the same period. For winter season at $R_{0.01} = 53.37$ mm/h, the DSD peak is closer to $62\,\mathrm{m}^{-3}\mathrm{mm}^{-1}$ at 1.665 mm bound. The orientations of the plotted graphs, for modified gamma and Weibull models in winter, suggest that the DSD may not be dependent on the drop concentration; this may due to the wholesome effect of the 'winter dry spell'. The winter season in Durban is characterised by general dryness and fewer occurrences of rainfall especially at the onset of the season.Finally, the season of spring at $R_{0.01} = 18.51$ mm/h has a DSD peak closer to $500\,\mathrm{m}^{-3}\mathrm{mm}^{-1}$ at 1.116 mm bound. For this season, the DSD seem closer to zero at the maximum distrometer diameter (5.373 mm). This may indicate near absence of rain drops at the diameter classes closer to the maximum diameter. The error statistics from the proposed Durban models are computed from the root mean square error (RMSE) using the drop-size PDF. The root mean square error is mathematically defined as:

$$RMSE = \sqrt{\frac{1}{N}\sum_{n=1}^{N}\left(y_{m,n} - y_n\right)^2} \tag{10}$$

In (10), $y_{m,n}$ and y_n both represent the nth sample from the proposed model data and actual measurements from the distrometer samples.

The fitting error statistics are computed for rainfall rates representing different DSD spectra within the bounds of our proposed model for Durban. The maximum number of samples, n, from our data is 20, corresponding to the number of distrometer channels. The model results for lognormal model (LGN), modified gamma model (MGM) and Weibull model (WBL) are presented per season in Tables 5(a) and 5(b) at different rainfall rates. Based on the error estimates for summer season, lognormal distribution has the least fitting errors with an average RMS error of 0.30 for all rainfall rates, in comparison with average RMS errors of 0.43 and 0.34, for modified gamma and Weibull distribution respectively. As earlier seen, the summer season has the highest density of rainfall samples for various regimes. Thus, the lognormal distribution is a preferable estimate of the measured rainfall drop-size PDF for summer season. For autumn, the Weibull and lognormal distribution both have the least fitting errors with an average RMS of 0.26. However, the lognormal model performs better than the Weibull model, particularly at rainfall rates above 10 mm/h. Thus, it would suffice to conclude that the proposed lognormal model is preferable for modelling rainfall drop-sizes beyond 10 mm/h for autumn season. The gamma distribution has the least fitting error

Table 5. (a) RMS fitting errors from the proposed summer and autumn seasonal DSD models for Durban. (b) RMS fitting errors from the proposed winter and spring seasonal DSD models for Durban.

(a)

Rainfall	**SUMMER**			**AUTUMN**		
rate (mm/h)	LGN	MGM	WB	LGN	MGM	WB
1	0.2981	0.5646	0.3782	0.6385	0.5756	0.4629
3	0.4087	0.3965	0.3264	0.4936	0.3715	0.2862
5	0.2143	0.3879	0.2792	0.2685	0.4170	0.2333
10	0.2657	0.4269	0.3302	0.1624	0.4128	0.2259
16	0.2635	0.2745	0.2159	0.2179	0.3411	0.1837
20	0.2645	0.3487	0.2755	0.1289	0.3590	0.1938
30	0.2597	0.4555	0.3732	0.2146	0.3986	0.2598
40	0.3329	0.4668	0.3815	0.1885	0.3785	0.2442
50	0.3675	0.5128	0.4283	0.1854	0.3303	0.2089
60	0.3261	0.4663	0.3843	0.1878	0.3553	0.2374
120				0.2194	0.4319	0.3356

(b)

Rainfall	**WINTER**			**SPRING**		
rate (mm/h)	LGN	MGM	WBL	LGN	MGM	WB
1	0.4627	0.2171	0.2492	0.6422	0.4799	0.4591
3	0.4360	0.1756	0.2482	0.2589	0.3195	0.2092
5	0.2983	0.1559	0.1372	0.3158	0.2976	0.2455
10	0.2823	0.1640	0.1866	0.2468	0.2669	0.2163
16	0.2923	0.1506	0.1626	0.1952	0.2527	0.2095
20	0.4298	0.1701	0.3157	0.1529	0.2857	0.2393
30	0.3180	0.0872	0.2028			
40	0.3598	0.1389	0.2588			
50	0.3261	0.2189	0.2591			
76	0.3273	0.1000	0.2185			

for the winter season with an average RMS error of 0.16; the model is seen to have a good fits at all sampled rainfall rates up to 76 mm/h. On the contrary, Weibull and lognormal distribution both have an average RMS of 0.22 and 0.35 respectively. Lastly, the Weibull model is seen to have the lowest fitting errors for spring season with an average RMS error of 0.26. The lognormal and gamma distribution in this season have very close RMS errors of 0.30 and 0.32 respectively.

The seasonal characteristics of rainfall DSD basically varies as observed in different models and their fitting errors. While the seasonal changes account for the fluctuations in the rainfall water volume, the coastal location in Durban may play a great role especially in the heterogeneity composition of rainfall drop-sizes. This missing gap may be subjected to further research for adequate understanding.

8. RAINFALL SPECIFIC ATTENUATION FOR SEASONAL CYCLES IN DURBAN

The extinction cross section (ECS) is the determinant parameter that allows for the estimation of 'interface' area of the arriving rain droplets due to the effects of droplet scattering. The Mie scattering theory is used alongside the results obtained from the computations of the complex refractive index of water, m, proposed by Liebe et al. [34]. The approach used in [34] employed the single and double Debye method conveniently catering for refractive indices of water for frequencies between 1 GHz and 1000 GHz. Our assumption is solely based on spherical shape for rainfall droplets at 20°C ambient temperature.

The ECS can be computed mathematically using the expression by Van de Hulst [35], given by:

$$Q_{ext}(D) = \frac{4\pi}{k^2} Re\{S(0)\} \tag{11}$$

where k is the wave number for all spherical sizes of radius, a, in mm.

In the Mie scattering theory [36], the real part of the forward scattering amplitude is used to determine the scattering parameters. By definition, the forward scattering amplitude is given from [35] as:

$$s(0) = \frac{1}{2} \sum_{n=1}^{\infty} (2n+1) [a_n(m,\alpha) + b_n(m,\alpha)] \tag{12}$$

where $a_n(m,\alpha)$ and $b_n(m,\alpha)$ correspond to the Mie scattering coefficients which are dependent on, m the complex refractive index of water, and α which depends on both the ambient temperature and droplet frequency.

The nth truncation of the infinite series in (12) can be determined from the works of Bohren and Huffman [37] and of Mulangu and Afullo [4]. The solution for nth truncated values of $a_n(m,\alpha)$ and $b_n(m,\alpha)$ of the forward scattering amplitude, $s(0)$, can be found using a combination of special spherical Bessel functions for spherical raindrops [38, 39]. Simulation at different water frequencies of 2 GHz, 10 GHz, 40 GHz, 60 GHz, 100 GHz, 400 GHz, 700 GHz and 1000 GHz are undertaken at 20°C as shown in Figure 5.

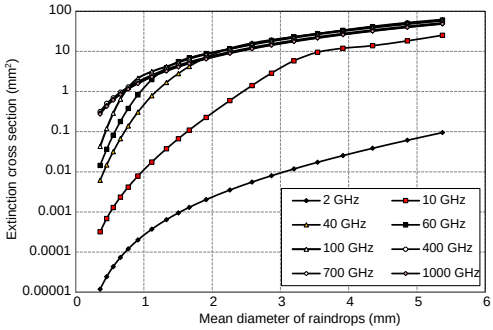

Figure 5. The plot of extinction cross section against rain droplet diameter at different water frequencies for 20°C ambient temperature.

By extension, the specific attenuation is given in [1] as:

$$A_s[\text{dB/km}] = 4.343 \times 10^{-3} \int_0^{\infty} N(D)\, Q_{ext}(D) dD \qquad (13)$$

where $N(D)$ is the rainfall drop-size distribution in $\text{m}^{-3}\text{mm}^{-1}$ and $Q_{ext}(D)$ is the extinction cross section with a unit of mm^2.

9. VARIATION OF SEASONAL SPECIFIC ATTENUATION

The variation of seasonal specific attenuation is conspicuously evident in the graphs displayed from Figures 6(a)–(d). It is observed that the Weibull DSD model has a higher specific attenuation estimates for all the seasons in Durban. Below 100 GHz, the autumn season at $R_{0.01} = 72.15$ mm/h is observed to have the highest estimates with an average fluctuation of about 2 dB/km when compared to summer season. The seasons of winter and spring are both predicted to witness the lowest figures of specific attenuation at 53.37 mm/h and 18.51 mm/h respectively. Also, the estimates for winter season are higher at 100 GHz when compared with that of the spring season. In addition, above 100 GHz, the summer season has the highest estimates when compared with other seasons. Although, it appears that summer and autumn have similar estimates with the lognormal and gamma DSD models especially at frequencies closer to 1 THz. On the contrary, the winter and spring seasons have the lowest estimates above 100 GHz. The spring season is, however, observed to have higher estimates than the winter season; this is possibly as a result of high density of rainfall drops in spite of its lower value of $R_{0.01}$ of 18.51 mm/h in comparison with winter at 53.37 mm/h.

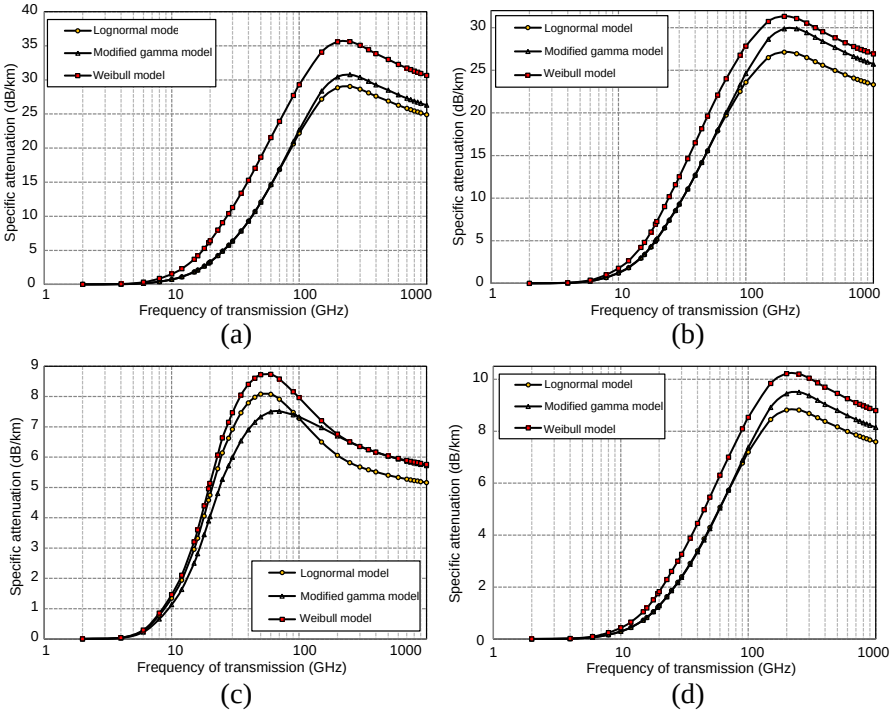

Figure 6. Specific attenuation variation for the proposed models between 2 GHz and 1000 GHz for different seasons in Durban. (a) Summer season at $R_{0.01} = 50.48$ mm/h. (b) Autumn season at $R_{0.01} = 72.15$ mm/h. (c) Winter season at $R_{0.01} = 53.37$ mm/h. (d) Spring season at $R_{0.01} = 18.51$ mm/h.

An overall examination of the variation in the specific attenuation for all the proposed models at selected frequencies and respective $R_{0.01}$ is undertaken. At 12 GHz: summer season estimates ranges from 0.89 dB/km to 2.3 dB/km; autumn season from 1.44 dB/km to 2.65 dB/km; winter season from 1.272 dB/km to 2.10 dB/km; spring season from 0.35 dB/km to 0.65 dB/km. At 60 GHz: summer season estimates ranges from 12.54 dB/km to 21.53 dB/km; autumn season from 14.45 dB/km to 22.11 dB/km; winter season from 5.93 dB/km to 8.13 dB/km; spring season from 6.20 dB/km to 6.31 dB/km. At 400 GHz: summer season estimates ranges from 27.60 dB/km to 33.84 dB/km; autumn season from 25.60 dB/km to 29.53 dB/km; winter season from 5.51 dB/km to 6.17 dB/km; spring season from 8.38 dB/km to 9.69 dB/km.

Table 6. Comparison of derived κ and α coefficients from the seasonal DSD models with ITU models at 2.5 GHz, 25 GHz, 40 GHz and 100 GHz in Durban.

SEASONAL	FREQUENCY (GHz)							
	2.5		25		40		100	
	κ	α	κ	α	κ	α	κ	α
SUMMER	0.0004	0.917	0.0902	1.0169	0.2384	0.9338	1.0947	0.7673
AUTUMN	0.0004	0.917	0.0924	1.0251	0.2324	0.935	0.9555	0.7493
WINTER	0.0004	0.8115	0.146	0.9077	0.261	0.8286	0.5843	0.639
SPRING	0.0003	1.0385	0.0809	1.1852	0.1979	1.0631	0.7762	0.8194
ITU-R (H)	0.0001321	1.1209	0.1571	0.991	0.4431	0.8673	1.3671	0.6815
ITU-R (V)	0.0001464	1.0085	0.1533	0.9491	0.4274	0.8421	1.3680	0.6765

Based on seasonal variability, our investigation has shown that the two seasons of summer and autumn respectively account for the highest specific attenuation in Durban, with interchangeable roles, below 100 GHz and above 100 GHz. On the other hand, the seasons of winter and spring do have lower specific attenuation, with interchangeable roles, below 100 GHz and above 100 GHz.

Furthermore, a derivation of seasonal κ and α coefficients for specific attenuation, using regression fitting technique, from the best proposed models is undertaken. The rainfall DSD model with the least RMS fitting errors at sampled rainfall rates, as earlier seen in Section 5, is considered as the default model for each of the four seasons in Durban. Therefore, the models used for the specific attenuation derivation are: lognormal model for summer and autumn seasons, gamma model for winter season and Weibull model for spring season. Table 6 shows the results of the specific attenuation coefficients derived from proposed statistical model with the lowest fitting errors, compared with ITU-R models for horizontal and vertical polarization [6], at selected frequencies. These frequencies were selected based on their popularity in the deployment of wireless networks, for example, 2.5 GHz is used as proprietary industrial, scientific and medical (ISM) band, 25 GHz utilized in local multipoint distribution service (LMDS) and 40 GHz for Ka-band deployment in satellite networks. Generally, signal propagation at 100 GHz, particularly for terrestrial links, is cumbersome and may result in large fade margins. This is so because the effects of atmospheric influences such as water vapour and oxygen are intense at this frequency.

A closer look at the results in Table 6 show the significant similarity in the power-law coefficients derived for the specific

attenuation in summer and autumn seasons. Also, a slight deviation in the coefficients is observed as the frequency increases towards 100 GHz at all rainfall rates for both seasons. The specific attenuation coefficients for spring season is seen to differ considerably from that of summer and autumn season irrespective of frequency. The spring season has the lowest scale factor, κ, and highest shape factor, α, when compared with other seasons except at 100 GHz. Again, a deviation in the coefficients is noted as the frequency increases towards 100 GHz for this season. It does appear the spring season may indeed be affected by the preponderance of lower rainfall rates and poor rainfall occurrences. For the ITU-R models, lower values of κ and higher values of α, are noted for all seasons at 2.5 GHz. Broadly speaking, the ITU-R models (for both horizontal and vertical polarization) are observed to have higher values of κ at 25 GHz, 40 GHz and 100 GHz irrespective of the season. On the contrary, the ITU-R models are seen to have lower values of α at 25 GHz, 40 GHz and 100 GHz, with the exception of winter season.

Obviously, it is noted that the specific attenuation predicted at similar rainfall rates may indeed depend on the seasonal effects encountered by transmitted waves in the propagation medium. This suggests that similar rainfall rates may yield different rainfall attenuation in different seasons, as seen in the local example of Durban.

10. CONCLUSION

The level of rainfall attenuation experienced at a locality is a subject of climatic factors which influence the seasonal patterns of rainfall microstructural processes. In this study, rainfall specific attenuation was investigated based on the seasonal dynamics of rainfall rate and rainfall drop-sizes using a two-year rainfall measurement from J-W distrometer for a subtropical site, Durban. With regards to the development of rainfall DSD models for seasonal relationship — the lognormal, modified gamma and Weibull distributions — were considered. The best fits for various seasons are as thus: lognormal distribution for summer and autumn, gamma distribution for winter and Weibull distribution for spring season. The computation of specific attenuation from seasonal rainfall DSD has shown that the summer and autumn seasons in Durban may witness intense attenuation, and hence, destructive signal degradation effects as suggested by [9]. Conversely, the winter and spring seasons are predicted to experience lesser rainfall attenuation effects for the same location. Also, it is observed that similar values of rainfall rates might not yield the same rainfall attenuation figures because the processes and mechanics of

rainfall may be dependent on the annual water volume contribution for each season. This, in part, may explain the seasonal variations in the compared specific attenuation at different frequencies. While the issue of variations in rain cell growth dynamics cannot be completely account for, there is a need for continual and long-term research of seasonal effects on rainfall attenuation as this can help provide appropriate effective fade countermeasures for terrestrial link budget. This should be undertaken to yield a much more reliable database of rainfall microstructural statistics for microwave applications. In summary, it is imperative for microwave engineers to take necessary precautions by allocating reasonable radio resources for link design and optimization, by considering the seasonal effects of rainfall attenuation.

ACKNOWLEDGMENT

The authors would like to acknowledge the Centre for Engineering Postgraduate Studies (CEPS) of the University of KwaZulu-Natal, Durban for their assistance and resources provided for this research.

REFERENCES

1. Ajayi, G. O., S. Feng, S. M. Radicella, and B. M. Reddy (Eds.), *Handbook on Radiopropagation Related to Satellite Communications in Tropical and Subtropical Countries,* ICTP, Trieste, 1996.
2. Crane, R. K., *Electromagnetic Wave Propagation Through Rain*, John Wiley, New York, 1996.
3. Green, H. E., "Propagation impairment on Ka-band SATCOM links in tropical and equatorial regions," *IEEE Trans. Antennas Propagat.*, Vol. 46, No. 2, 31–45, April 2004.
4. Mulangu, C. T. and T. J. Afullo, "Variability of the propagation coefficients for microwave links in Southern Africa," *Radio Sci.*, Vol. 44, 2009.
5. Li, L., T. Yeo, P. Kooi, and M. Leong, "An efficient calculation approach to evaluation of microwave specific attenuation," *IEEE Trans. Antennas Propag.*, Vol. 48, No. 8, 1220–1229, 2000.
6. ITU-R, "Specific attenuation model for rain for use in prediction methods," *ITU-R Rec. P.838-3*, Geneva, 2005.
7. ITU-R, "Propagation data and prediction methods for the design of terrestrial line-of-sight systems," *ITU-R Rec. P.530-13,*, Geneva, 2009.
8. ITU-R, "Characteristics of precipitation for propagation modelling," *ITU-R Rec. P.837-1, 2, 3, 4, 5,* Geneva, 2007.

9. Odedina, M. O. and T. J. Afullo, "Characteristics of seasonal attenuation and fading for line-of-sight links in South Africa," *Proc. of SATNAC*, 203–208, Wild Coast Sun, South Africa, September 2008.
10. Marcus, M. and B. Pattan, "Millimeter wave propagation-spectrum management implications," *IEEE Microwave Mag.*, Vol. 6, No. 2, 56–61, June 2005.
11. Yeo, T. S., P. S. Kooi, and M. S. Leong, "A two-year measurement of rainfall attenuation of CW microwaves in Singapore," *IEEE Trans. Antennas Propagat.*, Vol. 41, No. 6, 709–712, June 1993.
12. Das, S., A. Maitra, and A. K. Shukla, "Rain attenuation modeling in the 10–100 GHz frequency using drop size distributions for different climatic zones in tropical India," *Progress In Electromagnetics Research B*, Vol. 25, 211–224, 2010.
13. Rainfall, Climate, Durban, South Africa, accessed at www.ceroi.net/ reports/durban/drivers/Climate/rainfall.htm.
14. South Africa Weather and Climate, accessed at www.sa-venues.com/no/weather.htm.
15. Fashuyi, M .O., P. A. Owolawi, and T. O. Afullo, "Rainfall rate modelling for LoS radio systems in South Africa," *Trans. of South African Inst. of Elect. Engineers (SAIEE)*, Vol. 97, 74–81, 2006.
16. Odedina, M. O. and T. J. Afullo, "Modeling of rain attenuation of terrestrial LOS radio link systems in South Africa," *Proc. of SATNAC Conf.*, Sugar Beach Resort, Mauritius, 2007.
17. Owolawi, O. A., "Rain rate probability density evaluation and mapping for the estimation of rain attenuation in South Africa and surrounding Islands," *Progress In Electromagnetic Research*, Vol. 112, 155–181, 2011.
18. Alonge, A. A. and T. J. Afullo, "Estimation of parameters for lognormal rainfall DSD model for various rainfall types in Durban," *Proc. of SATNAC Conf. 2011*, East London, South Africa, September 2011.
19. Afullo, T. J. O., "Raindrop size distribution modeling for radio link design along the eastern coast of South Africa," *Progress In Electromagnetic Research B*, Vol. 34, 345–366, 2011.
20. Odedina, M. O. and T. J. Afullo, "Determination of rain attenuation from electromagnetic scattering by spherical raindrops: Theory and experiment," *Radio Sci.*, Vol. 45, 2010.

21. Owolawi, P. A., "Raindrop size distribution model for the prediction of rain attenuation in Durban," *PIERS Online*, Vol. 7, No. 6, 516–523, 2011.
22. Alonge, A. A. and T. J. Afullo, "Rainfall rate modeling for various rainfall types in South Africa," *Proc. IEEE AFRICON Conf.*, 1–6, Livingstone, Zambia, ISBN 978-1-61284-991-1, September 2011.
23. Distrometer product description at www.distromet.com.
24. Bartholomew, M. J., "Disdrometer and tipping bucket raingauge handbook," DOE/SC-ARM/TR-079, ARM Climate Research Facility, December 2009.
25. Ajayi, G. O. and R. L. Olsen, "Modeling of a tropical raindrop size distribution for microwave and millimeter wave applications," *Radio Sci.*, Vol. 20, No. 2, 193–202, April 1985.
26. Adimula, I. A. and G. O. Ajayi, "Variation in raindrop size distribution and specific attenuation due to rain in Nigeria," *Ann. Telecom*, Vol. 51, Nos. 1–2, 87–93, 1996.
27. Timothy, K. I., J. T. Ong, and E. B. L. Choo, " Raindrop size distribution using method of moments for terrestrial and satellite communication applications in Singapore," *IEEE Trans. Antennas Propagat.*, Vol. 50, 1420–1424, October 2002.
28. Atlas, D. and C. W. Ulbrich, "The physical basis for attenuation-rainfall relationships and the measurement of rainfall parameters by combined attenuation and radar methods," *J. Rech. Atmos.*, Vol. 8, 275–298, 1974.
29. Ulbrich, C. W., "Natural variation in the analytical form of the raindrop size distribution," *J. of Climate and Applied Meteor.*, Vol. 23, 1764–1775, 1983.
30. Sekine, M., C. Chen, and T. Musha, "Rain attenuation from log-normal and Weibull raindrop-size distribution," *IEEE Trans. Antennas Propag.*, Vol. 35, No. 3, 358–359, March 1985.
31. Jiang, H., M. Sano, and M. Sekine, "Weibull raindrop-size distribution and its application to rain attenuation," *IEE Proc. Microw. Antennas Propag.*, Vol. 144, No. 3, 197–200, June 1997.
32. Kozu, T. and K. Nakamura, "Rainfall parameter estimation from dual-radar measurements combining reflectivity profile and path-integrated attenuation," *J. of Atmos. and Oceanic tech.*, 259–270, 1991.
33. Murthy, D. N., M. Xie, and R. Jiang, *Weibull Models*, 50–58, 68–74, John Wiley and Sons Inc., New York, 2004.
34. Liebe, H. J., G. A. Hufford, and T. Manabe, "A model for the complex permittivity of water at frequencies below 1 THz," *Inter.*

J. of Infrared and Millimeter Waves, Vol. 12, No. 7, 659–678, 1991.

35. Van de Hulst, H. C., *Light Scattering by Small Particles*, John Wiley and Sons Inc., New York, 1957.
36. Mie, G., "Beiträge zur optik trüber medien, speziell kolldaler metallösungen," *Ann. Phys.*, Vol. 25, 377–445, 1908.
37. Bohren, C. F. and D. R. Huffman, *Absorption and Scattering of Light Particles*, John Wiley, Wienheim, 2004.
38. Mätzler, C., "Drop-size distributions and Mie computation," *IAP Res. Rep. 2002-16*, University of Bern, Bern, November 2002.
39. Odedina, M. O. and T. J. Afullo, "Analytical modeling of rain attenuation and its application to terrestrial LOS links," *Proc. of SATNAC*, Royal Swazi Spa, Swaziland, 2009.